Elimination of standing wave effects in ultrasound radiation force excitation in air using random carrier frequency packets

Thomas M. Huber,[a] Nathaniel M. Beaver, and Justin R. Helps
Physics Department, Gustavus Adolphus College, 800 College Avenue, Saint Peter, Minnesota 56082

(Received 28 October 2010; revised 27 July 2011; accepted 2 August 2011)

The ultrasound radiation force has been used for noncontact excitation of devices ranging from microcantilevers to acoustic guitars. For ultrasound radiation force excitation, one challenge is formation of standing waves between the ultrasound transducer and the device under test. Standing waves result in constructive/destructive interference causing significant variations in the intensity of the ultrasound field. The standing-wave induced intensity variations in the radiation force can result from minor changes in the transducer position, carrier frequency, or changes in the speed of sound due to changes in ambient temperature. The current study demonstrates that by randomly varying the ultrasound carrier frequency in packets, it is possible to eliminate the negative consequences resulting from the formation of standing waves. A converging ultrasound transducer with a central frequency of 550 kHz was focused onto a brass cantilever. The 267 Hz resonance was excited with the ultrasound radiation force with a carrier frequency that randomly varied between 525 kHz to 575 kHz in packets of 10 cycles. Because each packet had a different carrier frequency, the amplitude of standing wave artifacts was reduced by a factor of 20 compared to a constant frequency excitation of 550 kHz. [DOI: 10.1121/1.3628336]

PACS number(s): 43.25.Gf, 43.35.Yb, 43.20.Ks, 43.25.Qp [TDM] Pages: 1838–1843

I. INTRODUCTION

Recent studies have demonstrated that ultrasound radiation force excitation[1,2] can be used as a noncontact alternative to mechanical excitation for a wide range of devices in air ranging from reed organ pipes,[3] to hard drive suspensions,[4] microcantilevers,[5] and the face of an acoustic guitar.[6] In water, ultrasound radiation force excitation has been used for detection of flaws in composite plates,[7] materials properties,[8] and for medical imaging.[9–11] For ultrasound radiation force experiments, a pair of ultrasound frequencies are emitted by a transducer. These two frequencies are symmetric around a carrier frequency, and the ultrasound radiation force causes excitation at the difference frequency between the sidebands.

In experiments that use ultrasound radiation force for excitation, one problematic issue is the development of standing waves between the transducer and the device under test. Development of standing waves can cause the amplitude of vibration resulting from the radiation force to vary by nearly a factor of two.[12] For standing waves, the difference between constructive and destructive interference occurs when there is a variation of a quarter of the ultrasound wavelength between the transducer and the surface of the device under test. Thus, minor changes in the transducer-to-device spacing or carrier frequency can lead to transitions from constructive to destructive interference. Substantial changes in amplitude can also result from minor variations in the ambient temperature, because the speed of sound in air is a function of temperature. This temperature dependence leads to both short-duration fluctuations and long-term drifts in the vibration amplitude.

In previous experiments, several methods have been used to eliminate standing wave formation between an ultrasound transducer and surface. One method was to orient the ultrasound transducer at an angle relative to the surface.[13] The difficulty with this technique is that it only works if the device under test is planar; for other devices, portions of the device may reflect ultrasound back to the transducer, which is a situation that allows standing waves to develop. Alternately, to mitigate the problem of standing waves for ultrasound experiments in water, recent studies have used variations in the ultrasound waveform, including chirp variation in the ultrasound carrier frequency,[12] random variations in the carrier frequency,[14,15] or phase-shift variations.[16] These methods for varying the carrier waveform result in discontinuities in the waveform or its time derivative, which may lead to artifacts when they are used to drive the ultrasound transducer.

The current study describes a technique that uses variations in the carrier frequency to eliminate standing waves without introducing discontinuities in the waveform or its time derivative. In this technique, the carrier frequency is randomly chosen within a specified range, and this carrier frequency is maintained for an integer number of carrier cycles. This can be thought of as a single packet with a constant carrier frequency; at the end of an integral number of carrier cycles in this packet, a new carrier frequency is selected. Because each of these packets has a different carrier frequency, there is not a systematic constructive or destructive interference between successive packets or their reflections.

In addition to eliminating the transducer position and carrier frequency sensitivity, carrier frequency packets effectively eliminate amplitude variations and drift that are commonly observed in radiation force experiments in air. Measurements in the current study indicate that these are likely due to

[a]Author to whom correspondence should be addressed. Electronic mail: huber@gac.edu

 0001-4966/2011/130(4)/1838/6/$30.00

temperature/density fluctuations of the air that can result from localized air currents. These variations in the amplitude of vibration are observed with timescales anywhere from fractions of a second to several hours.[17] These vibration amplitude variations have not been discussed in previous experiments performed in water.[12,14–16] It is likely that the volumes used in water-based experiments are more homogeneous in temperature and density than air inside of a room.

II. THEORY

A. Ultrasound radiation force excitation in air

As with many ultrasound radiation force excitation applications,[18] a single ultrasound transducer produces a dual sideband-suppressed carrier (DSB-SC) velocity potential consisting of a pair of sine waves with frequencies of $f_a = f_c - f_m/2$ and $f_b = f_c + f_m/2$ symmetric about a carrier frequency f_c.[1–3] The acoustic radiation force is proportional to the square of the velocity potential.[1,19,20] Of importance for the current study is the component of the radiation force at the difference of the frequencies (alternately named the modulation frequency) $f_m = (f_b - f_a)$. The conventional method for writing the velocity potential, $\Phi(t)$, of amplitude Φ_0, as a function of time t for a DSB-SC waveform is

$$\Phi(t) = \Phi_0 \cos[2\pi(f_c - f_m/2)t] + \Phi_0 \cos[2\pi(f_c + f_m/2)t]. \tag{1}$$

To better understand the algorithm used in the current paper, it is helpful to isolate the carrier and modulation frequencies by rewriting Eq. (1) in a mathematically equivalent form as

$$\Phi(t) = 2\Phi_0 \cos(2\pi f_c t) \cos[2\pi(f_m/2)t]. \tag{1a}$$

As detailed in Ref. 21, the square of the DSB-SC velocity potential of Eq. (1) results in a radiation force $\boldsymbol{F_R}(t)$,

$$\boldsymbol{F_R}(t) = \boldsymbol{F_S} + \boldsymbol{F_D} \cos(2\pi f_m t) + \boldsymbol{F_{HF}}\{\cos(4\pi f_c t) + \cos[2\pi(2f_c - f_m)t] + \cos[2\pi(2f_c + f_m)t]\} \tag{2}$$

where $\boldsymbol{F}_S$ is a time-independent static radiation force, $\boldsymbol{F}_D$ is the amplitude of the radiation force at the difference frequency f_m, and $\boldsymbol{F}_{HF}$ is the amplitude of the high-frequency terms in the radiation force. For the current experiment, where an ultrasound carrier frequency f_c on the order of 550 kHz is used to excite audio-frequency resonances of a brass cantilever, these high-frequency components of the radiation force are in the MHz frequency range and are eliminated using a low-pass filter. The only time-varying component of interest for the current experiment is the radiation force component $\boldsymbol{F}(t)$ at the difference frequency f_m,

$$\boldsymbol{F}(t) = \boldsymbol{F_D} \cos(2\pi f_m t). \tag{3}$$

For the remainder of this paper, discussions of the radiation force will refer only to this time-varying component with frequency f_m. The amplitude, $\boldsymbol{F}_D$, of this radiation force depends on a number of factors, including the magnitude of the intensity of the ultrasound incident on the surface, as well as specific characteristics of the surface. The effects of standing waves manifest themselves by substantial variations in $\boldsymbol{F}_D$ caused by changes in ambient air temperature, carrier frequency, and transducer to device separation.

B. Random carrier frequency packets

Instead of keeping a constant carrier frequency, in the current experiment, the carrier frequency is randomly changed while keeping the modulation frequency, f_m, constant. The result is a series of "packets," each with a different carrier frequency. Because the carrier frequencies of packets are not correlated, the reflected waves do not add constructively or destructively to form standing waves. In particular, the following algorithm is used to generate waveforms:

1. Before waveform generation begins, a central carrier frequency f_0 and frequency range f_W are specified; the carrier frequencies used for the waveform are randomly selected in the range $f_0 - f_W/2 < f_c < f_0 + f_W/2$. The other parameter specified is the integer N_C, which is the number of cycles in each packet generated before a new carrier frequency is selected.
2. The time variable is initialized to $t = 0$. The starting time for each packet is specified by t', so for the first packet, t' is initialized to 0.
3. At the start of each packet, which occurs at a time t', a frequency f_c is randomly chosen in the range from $f_0 - f_W/2$ to $f_0 + f_W/2$.
4. A phase constant

$$\varphi_c' = -2\pi f_c t' \tag{4}$$

is calculated. This insures that at time $t = t'$, the total phase of the carrier signal $2\pi f_c t + \phi_c'$ is zero at the start of each packet.
5. The waveform is generated

$$\Phi(t) = 2\Phi_0 \cos(2\pi f_c t + \varphi_c') \cos[2\pi(f_m/2)t] \tag{5}$$

for a time interval from $t' \le t < t' + \Delta t'$, where $\Delta t' = N_C/f_c$.
6. When the time interval of $\Delta t' = N_C/f_c$ has elapsed following a frequency change, a total of N_C cycles of the carrier frequency f_c will have been generated in the packet, and the total phase of the carrier signal will once again be zero. The start of the next packet will be at a new time given by adding $\Delta t'$ to the previous packet start time; thus t' is replaced by $t' + \Delta t'$. The program then returns to step 3 of the algorithm to select a new random frequency f_c and continue the waveform generation process.

With this algorithm the frequency transitions occur at the peak of the cosine waveform. This insures that both the waveform and its time derivative are continuous when there is a frequency transition. Figure 1 shows a sample time series of the carrier waveform when $N_C = 3$; in other words, each packet has three full cycles at one carrier frequency, and then a jump to another frequency. To clearly illustrate the changes between packets in Fig. 1, a dashed line has

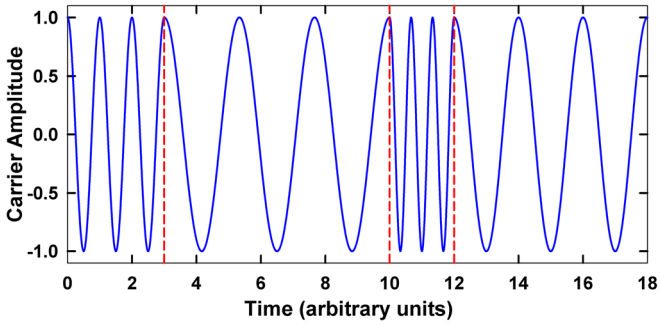

FIG. 1. (Color online) Illustration of a sequence of random carrier frequency packets; dashed lines indicate the time when the carrier frequency changed. Transitions occur at the maximum value of the cosine to insure continuity of the waveform and its time derivative.

been included between packets, and the changes are accentuated by having the frequency change by about a factor of 2 in each successive packet. In the actual experiments performed, the changes in frequency were not nearly as abrupt because the random change in frequency was less than 10% of the carrier frequency. The signal that is sent to the transducer is the product of the carrier waveform by the sinusoidal modulation waveform, calculated according to Eq. (5).

III. EXPERIMENT SETUP

To produce the ultrasound, a MicroAcoustic Instruments (Gatineau, Quebec, Canada) broadband air-coupled ultrasound transducer with a focal length of 70 mm, 10 mm depth of field, and a spot diameter of about 2 mm was used. The ultrasound transducer had a center frequency of about 550 kHz with a bandwidth of over 300 kHz,[17] so its response is essentially flat over the frequency range used for this experiment. The transducer was mounted on a Newport 423 translation stage (Irvine, CA) that was moved using a computer-controlled Zaber Technologies Incorporated, T-NA08A25 linear actuator (Vancouver, British Columbia, Canada) with 0.05 μm resolution. The transducer was focused at normal incidence near the free end of an 8.0 mm $\times$ 29.4 mm $\times$ 0.1 mm brass cantilever clamped at one end. The cantilever used for the experiment had a fundamental frequency of 267 Hz and Q-factor of 215 $\pm$ 5.

Waveforms were output from a 4-channel Strategic Test UF2e-6022 60 MHz Arbitrary Waveform Generator PCI express board (Stockholm, Sweden). The DSB-SC waveform generated for the ultrasound transducer had a 800 ms duration, a sampling rate of 60 MSamples/s, and a modulation frequency of $f_m = 267$ Hz. This waveform was produced using a Microsoft VISUAL C++ program to calculate either Eq. (2) for a fixed carrier frequency or Eq. (5), and the algorithm described in Sec. II B for random carrier packets. This 800 ms waveform was uploaded to the Strategic Test board and was repeatedly cycled through one of the DAC board output channels. This waveform was amplified using an ENI-240L RF amplifier to about 70 Vrms. Another DAC output channel continuously cycled a simple cosine waveform of frequency $f_m = 267$ Hz; this cosine waveform was the reference signal for the lock-in amplifier.

To determine the vibration of the cantilever, a Polytec PSV-400 Scanning Laser Doppler Vibrometer (Waldbronn, Germany) was focused near the free end of the cantilever. The vibrometer was set to a 1 mm s^{-1} V^{-1} scaling; a 100 kHz low-pass filter eliminated signals due to vibrations near 550 kHz that were generated by the ultrasound sidebands and high-frequency radiation force terms that were in the MHz frequency range. The vibrometer analog output signal was routed into a Zurich Instruments HF2LI Lock-In Amplifier (Zurich, Switzerland) with a 71 ms time constant; the reference signal was the $f_m = 267$ Hz cosine signal produced with the Strategic Test DAC board. The lock-in amplifier was used to sample each measurement of vibration amplitude multiple times with a time delay between each sample that was equal to twice the time constant. The mean and standard deviation of the multiple samples were calculated in the complex plane; plotted data points in subsequent graphs were the mean and standard deviation of the average magnitude of the vibration amplitude.

The experiment was performed in a laboratory that has double-wall construction to acoustically isolate this room from external noise sources. The air handling system for this room continuously circulated a small volume of air through floor vents, with increased heated airflow when requested by the room thermostat. The temperature in the room was monitored in several locations using National Semiconductor LM35 Precision Centigrade Temperature Sensors (Santa Clara, CA). The room averaged 20.5 $\pm$ 0.5 °C, with excursions from the average up to about 1 °C depending on the state of the air-handling system. To eliminate air currents and temperature fluctuations, a 0.59 m $\times$ 0.59 m $\times$ 0.55 m corrugated cardboard box could be placed over the optical isolation table where the experiment was set up; this would enclose the transducer and cantilever. The only opening in this enclosure where air could be exchanged was a 30 mm square cutout where the vibrometer beam entered. The temperature inside the enclosure was monitored with a LM35 temperature sensor located 20 mm from the cantilever.

IV. RESULTS

A. Standing wave effects resulting from variations in ambient air temperature

The resonance frequency of the brass cantilever was measured using the vibrometer, with excitation from a mechanical shaker, to be 267 Hz with a Q-factor of 215 $\pm$ 5. An ultrasound excitation measurement was also performed with the carrier frequency fixed at $f_c = 550$ kHz; for this preliminary measurement the transducer was mounted at roughly a 45 degree angle relative to the surface to minimize formation of standing waves. As with previous studies,[3] the ultrasound excitation and mechanical shaker gave the same values, within experimental uncertainty, for the resonance frequency and Q-factor.

The transducer was then repositioned such that it was normal to the surface; this was a situation that allowed formation of standing waves. Figure 2 shows repetitive measurements of the 267 Hz velocity amplitude; for this figure, each data point was an average of three samples, and data

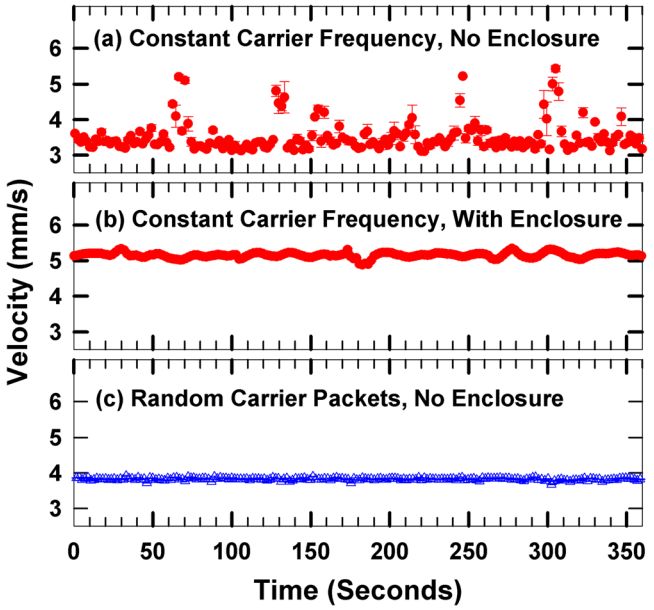

FIG. 2. (Color online) Measurements of the 267 Hz velocity amplitude taken every 2 s: (a) substantial fluctuations in the amplitude were observed when carrier frequency was a constant value of 550 kHz; (b) fluctuations in velocity amplitude were reduced by surrounding the apparatus with an enclosure to reduce temperature variations; (c) substantial suppression of the fluctuations even without the enclosure by using random carrier packets.

points were taken every 2 s. In Fig. 2(a), the carrier frequency was kept constant at $f_c = 550$ kHz without any random jumps in frequency. This plot showed a number of significant fluctuations due to temperature variations and air currents in the room. To demonstrate that temperature variations were the source of these fluctuations, in Fig. 2(b), the cardboard enclosure was placed over the apparatus to isolate it from air currents. After about 1 h, the air temperature measured in the enclosure reached a steady value. The velocity amplitude fluctuations observed in Fig. 2(a) were greatly reduced in Fig. 2(b) because the enclosure virtually eliminated air currents and temperature changes during the duration of the run. While this enclosure reduced short-term amplitude variations, there were still long-term drifts that occurred over the course of several hours due to changes in room temperature, such as when the building's air-handling regulation changed between daytime and nighttime requirements. Standing waves were not eliminated by placing the enclosure over the apparatus; instead the enclosure reduced the fluctuations and drift in the vibration amplitude that were due to air currents and temperature changes.

The random carrier packet method was used to eliminate the standing waves and the resulting fluctuations in vibration amplitude. For the data set shown in Fig. 2(c), the cardboard enclosure was removed so the apparatus experienced the same type of temperature fluctuations that were present in Fig. 2(a). The carrier frequency packets were generated in a range of $f_W = 50$ kHz around the central carrier frequency of $f_0 = 550$ kHz using the algorithm described in Sec. II B. During each packet, the carrier frequency was held constant for $N_c = 10$ complete cycles of the carrier. Because standing waves did not form, the fluctuations present in Fig. 2(a) were eliminated using this method.

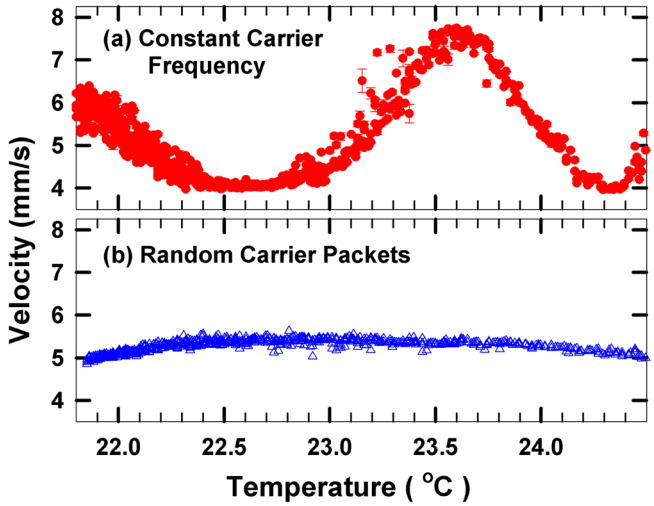

FIG. 3. (Color online) Measurements of the 267 Hz velocity amplitude as a function of ambient temperature: (a) large temperature dependent fluctuations were present when the carrier frequency was a constant value of $f_C = 550$ kHz; (b) these large fluctuations were suppressed when the carrier frequency was varied using random carrier packets.

Figure 3 shows an even more dramatic demonstration of the efficacy of using random carrier packets to suppress the temperature-dependent standing wave variations. For these plots, the enclosure was placed over the apparatus along with a 40 W incandescent light bulb to heat the air inside the enclosure. When the temperature in the enclosure reached about 25 °C, the bulb was turned off, and the temperature and amplitude of vibration of the cantilever were recorded every 2 s. After about 1 h, the temperature decreased to about 22 °C. In Fig. 3(a), the carrier frequency was kept constant, so standing waves between the transducer and cantilever formed. As the temperature decreased, the amplitude of the vibration of the cantilever varied by nearly a factor of two due to changes from constructive to destructive interference. Using the speed of sound as approximately $v = 331.3 + 0.6T_C$ where T_C is the temperature in centigrade,[22] a temperature change of about 1.3 °C would result in a change of a quarter of a cycle of a 550 kHz frequency in the 70 mm distance between the cantilever and transducer. The data set in Fig. 3(a) was in qualitative agreement with this prediction because it showed cycles of constructive to destructive interference that occurred when the temperature dropped a few degrees Celsius. The asymmetry in this curve and the fact that the temperature difference between minima and maxima was less than 1.3 °C may be due to the non-equilibrium nature of this cool down experiment. Particularly at the start of the cool down period when the temperature was changing most rapidly, the sensor response time likely resulted in a lag between actual air temperature and the sensor's temperature reading.

The same thermal cycle was performed to produce the data set shown in Fig. 3(b); instead of using a constant carrier frequency, random carrier frequency packets ($f_0 = 550$ kHz, $f_W = 50$ kHz, $N_c = 10$ cycles) were used for the waveform. Because standing waves did not develop, the cyclic variations in constructive and destructive were not present, and only a weak temperature dependence was observed. The use of

random carrier packets minimized the extreme sensitivity of radiation force excitation to ambient temperature.

B. Standing wave effects resulting from changes in transducer position

Previous experiments in water have shown that standing wave interference resulted in substantial changes in pressure distributions when the spacing between the transducer and device under test was changed. Figure 4 demonstrated similar variations of the radiation force applied to the cantilever in air as the transducer position was varied by a small amount. The transducer was mounted on a computer-controlled linear translation stage at a nominal spacing of 70 mm between the transducer and the cantilever. The cardboard enclosure was placed over the cantilever and transducer to minimize temperature related fluctuations. The carrier frequency was fixed at 550 kHz, and the distance between the transducer and cantilever was decreased by a total of 1 mm in 40 increments. This 1 mm displacement was significantly smaller than the depth of field of the transducer; so, absent the formation of standing waves, the intensity of the ultrasound produced was constant over the range of displacement. At each transducer position, the amplitude of the cantilever vibration was sampled 15 times, and the average amplitude as a function of transducer displacement was plotted in Fig. 4(a). The graph clearly showed a cyclical variation in response similar to prior measurements of standing waves in water.[12,14–16] For standing waves, the displacement required for a transition from constructive to destructive interference was a quarter the wavelength of the ultrasound carrier, in this case $\lambda/4 = (343\ \text{m/s})/(4 \times 550\ \text{kHz}) = 156\ \mu\text{m}$. The variation of $164 \pm 7\ \mu$m between maxima and minima observed in Fig. 4(a) was consistent with the result expected for standing wave interference variations.

In previous works,[12,15,16] the effectiveness of suppression of standing waves was calculated using the standing wave ratio

$$R = (p_{max} - p_{min})/p_{ave}. \quad (6)$$

where p_{max}, p_{min}, and p_{ave} are the maximum, minimum, and average pressure measured at locations in water. For the current experiment, a similar ratio was calculated using the maximum, minimum, and average amplitudes of the vibration. For the measurements displayed in Fig. 4(a), the standing wave ratio was $R = 0.51 \pm 0.07$.

As shown in Fig. 4(b), the variations due to standing wave interference were virtually eliminated when random carrier frequency packets were used instead of a constant carrier frequency. For this plot, the standing wave ratio was $R = 0.018 \pm 0.002$, a reduction by a factor of 28 ± 5 from the case where the carrier frequency was constant. This plot shows that the amplitude of the response was nearly constant over the measured displacement of 1 mm. Thus, the use of random carrier packets to eliminate standing waves minimizes the sensitivity of ultrasound radiation force experiments to the transducer-to-device spacing.

C. Standing wave effects resulting from changes in carrier frequency

When standing waves formed between the transducer and surface, another negative effect was significant variations in the vibration amplitude as the carrier frequency was changed. For Fig. 5(a), the enclosure was placed over the apparatus to minimize temperature related fluctuations. The modulation frequency f_m was fixed at 267 Hz, and the carrier frequency was stepped from $f_C = 545$ to 555 kHz. For each carrier frequency, 15 samples of the vibration amplitude were averaged. The periodic variation observed in Fig. 5(a) were due to constructive and destructive interference as the carrier frequency was varied. For a 70 mm distance between the transducer and cantilever surface, and a carrier frequency in the vicinity of 550 kHz, the frequency change needed to add a quarter cycle of the carrier between the transducer and surface can be calculated to be 1.3 kHz. This was consistent with the measured spacing of 1.23 ± 0.05 kHz between maxima and minima on the graph. The standing wave ratio for this curve was $R = 0.53 \pm 0.08$.

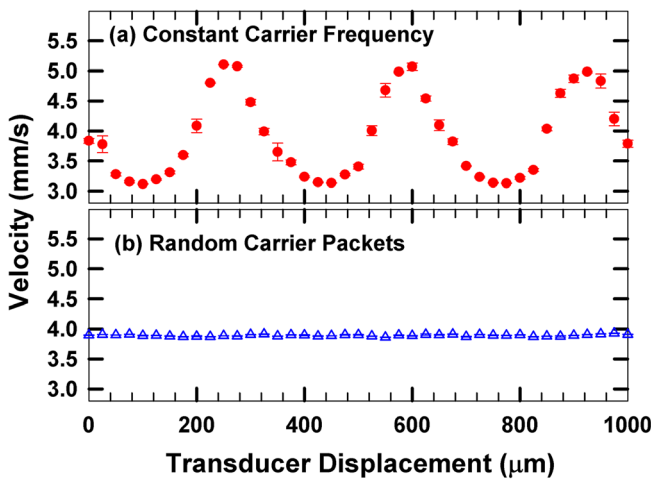

FIG. 4. (Color online) Measurements of the 267 Hz velocity amplitude as a function of the displacement of the transducer from its nominal 70 mm focal distance: (a) standing waves caused cyclic variations when the carrier frequency was kept constant; (b) the variations in amplitude were eliminated by varying the carrier frequency in random packets.

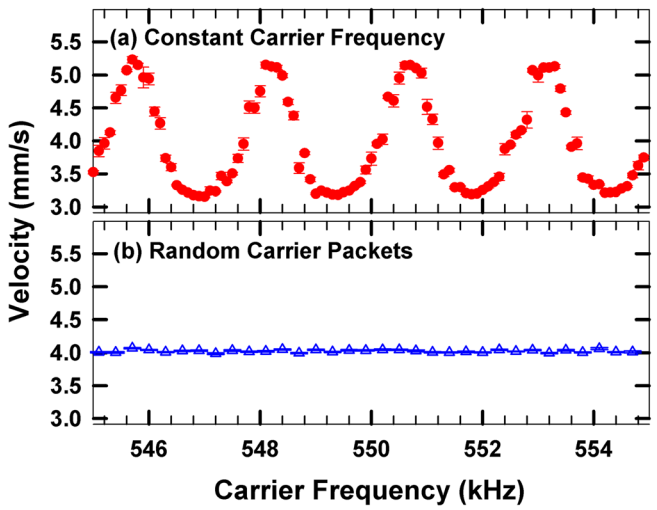

FIG. 5. (Color online) Measurements of the 267 Hz velocity amplitude as a function of the central carrier frequency: (a) standing waves caused cyclic variations when the carrier frequency was incremented from $f_C = 545$ to 555 kHz; (b) the variations in amplitude as a function of central carrier frequency f_0 were eliminated by varying the carrier frequency in random packets.

In Fig. 5(b), the sensitivity to carrier frequency was minimized with the use of carrier frequency packets. For this curve, the carrier packet parameters, $N_c = 10$ and $f_W = 50$ kHz, were held constant, and the central carrier frequency was stepped from $f_0 = 545$ to 555 kHz. This use of carrier frequency packets led to a reduction by a factor of 20 ± 3 in the standing wave ratio between Fig. 5(a) and the $R = 0.026 \pm 0.002$ value for Fig. 5(b).

To determine optimal values for the carrier packet parameters N_c and f_W, the carrier frequency measurements shown in Fig. 5(b) were repeated numerous times using different parameters. Tests were performed for many frequency widths, f_W, ranging from 1 kHz to 800 kHz.[17] For widths f_W smaller than about 3 kHz, the carrier frequencies of the packets were close enough that there was little reduction in the standing wave ratio from the value measured with a constant carrier frequency. Frequency widths from $f_W = 5$ kHz up to about $f_W = 25$ kHz gave partial cancellation of the standing wave effects, and using a random carrier width of larger than about $f_W = 50$ kHz did not significantly reduce the standing wave ratio beyond the results discussed in the current study. However, when the frequency width was larger than about 200 kHz, there was a significant reduction in amplitude of vibration of the cantilever because of the bandwidth of the transducer. It was also found that packet widths of anywhere from $N_c = 2$ to $N_c = 100$ gave nearly identical results. Therefore there was a broad range of packet parameters that effectively suppressed the formation of standing waves.

Other tests were performed to demonstrate that the random carrier packet technique was generally applicable. The same carrier packet parameters ($f_0 = 550$ kHz, $f_W = 50$ kHz, and $N_c = 10$) were used to suppress standing wave effects (temperature, transducer displacement, and carrier frequency dependence) for higher-order resonance frequencies of this cantilever at up to $f_m = 68$ kHz and for other brass cantilevers.[17] The same technique was used to suppress these effects when the device under test was the face of a classical guitar[6] with resonance frequencies ranging from 100 Hz to 3 kHz.

V. CONCLUSIONS

When using radiation force excitation in air with a constant carrier frequency, it was shown that formation of standing waves caused a critical sensitivity to variations in the transducer-sample spacing and carrier frequency used, as well as temperature dependent variations and drifts in response. The use of carrier frequency packets described in the current study effectively eliminated formation of standing waves, which mitigates the temperature dependence and related problems. This elimination of standing waves using random carrier packets greatly improves the repeatability of the radiation force excitation technique without reliance on precise device positioning and temperature control.

ACKNOWLEDGMENTS

The authors wish to acknowledge David Schindel, President of MicroAcoustic Instruments for assistance in construction and testing of the ultrasound transducer used in this experiment, and for helpful discussions. This material is based upon work supported by the National Science Foundation under Grant Nos. 0509993, 0900197, and 0959858. Any opinions, findings, and conclusions or recommendations expressed in this material are those of the author(s) and do not necessarily reflect the views of the National Science Foundation (NSF).

[1] M. Fatemi and J. F. Greenleaf, "Ultrasound-stimulated vibro-acoustic spectrography," Science **280**(5360), 82–85 (1998).
[2] M. Fatemi and J. F. Greenleaf, "Vibro-acoustography: An imaging modality based on ultrasound-stimulated acoustic emission," Proc. Natl. Acad. Sci. U.S.A. **96**(12), 6603–6608 (1999).
[3] T. M. Huber, M. Fatemi, R. Kinnick, and J. Greenleaf, "Noncontact modal analysis of a pipe organ reed using airborne ultrasound stimulated vibrometry," J. Acoust. Soc. Am. **119**(4), 2476–2482 (2006).
[4] T. M. Huber, D. Calhoun, M. Fatemi, R. R. Kinnick, and J. F. Greenleaf, "Noncontact modal testing of hard-drive suspensions using ultrasound radiation force," J. Acoust. Soc. Am. **118**, 1928 (2005).
[5] T. M. Huber, B. C. Abell, D. C. Mellema, M. Spletzer, and A. Raman, "Mode-selective noncontact excitation of microcantilevers and microcantilever arrays in air using the ultrasound radiation force," Appl. Phys. Lett. **97**(21) 214101 (2010).
[6] T. M. Huber, N. M. Beaver, and J. R. Helps, "Noncontact Modal Excitation of a Classical Guitar using Ultrasound Radiation Force Excitation," Exp. Tech. doi: 10.111/j.1747-1567.2011.00775.x.
[7] F. G. Mitri, J. F. Greenleaf, and M. Fatemi, "Comparison of continuous-wave (CW) and tone-burst (TB) excitation modes in vibro-acoustography: Application for the non-destructive imaging of flaws," Appl. Acoust. **70**(2), 333–336 (2009).
[8] J. C. Brigham, W. Aquino, F. G. Mitri, J. F. Greenleaf, and M. Fatemi, "Inverse estimation of viscoelastic material properties for solids immersed in fluids using vibroacoustic techniques," J. Appl. Phys. **101**(2) (2007).
[9] F. G. Mitri, B. J. Davis, J. F. Greenleaf, and M. Fatemi, "In vitro comparative study of vibro-acoustography versus pulse-echo ultrasound in imaging permanent prostate brachytherapy seeds," Ultrasonics **49**(1), 31–38 (2009).
[10] C. Pislaru, B. Kantor, R. R. Kinnick, J. L. Anderson, M. C. Aubry, M. W. Urban, M. Fatemi, and J. F. Greenleaf, "In vivo vibroacoustography of large peripheral arteries," Invest. Radiol. **43**(4), 243–252 (2008).
[11] A. Alizad, D. H. Whaley, J. F. Greenleaf, and M. Fatemi, "Critical issues in breast imaging by vibro-acoustography," Ultrasonics **44**, E217–E220 (2006).
[12] F. G. Mitri, J. F. Greenleaf, and M. Fatemi, "Chirp imaging vibro-acoustography for removing the ultrasound standing wave artifact," IEEE Trans. Med. Imaging **24**(10), 1249–1255 (2005).
[13] T. M. Huber, E. T. Ofstad, S. M. Barthell, A. Raman, and M. Spletzer, "Excitation of vibrational eigenstates of coupled microcantilevers using ultrasound radiation force," in *DETC2008: Proceedings of the ASME International Design Engineering Technical Conference and Computers and Information in Engineering Conference* (2009), Vol. 4, pp. 737–741.
[14] S. C. Tang and G. T. Clement, "Standing wave suppression for transcranial ultrasound by random-modulation," in *8th International Symposium on Therapeutic Ultrasound*, edited by E. S. Ebbini (American Institute of Physics, Melville, NY, 2009), Vol. 1113, pp. 3–7.
[15] S. C. Tang and G. T. Clement, "Standing-wave suppression for transcranial ultrasound by random modulation," IEEE Trans. Biomed. Eng. **57**(1), 203–205 (2010).
[16] S. C. Tang and G. T. Clement, "Acoustic standing wave suppression using randomized phase-shift-keying excitations," J. Acoust. Soc. Am. **126**(4), 1667–1670 (2009).
[17] See supplementary material at E-JASMAN-130-034110 for additional plots.
[18] M. Fatemi and J. F. Greenleaf, "Acoustic force generation by amplitude modulating a sonic beam," U.S. Patent No. 5,921,928 (1999).
[19] P. J. Westervelt, "The theory of steady forces caused by sound waves," J. Acoust. Soc. Am. **23**, 312–315 (1951).
[20] M. W. Urban, G. T. Silva, M. Fatemi, and J. F. Greenleaf, "Multifrequency vibro-acoustography," IEEE Trans. Med. Imaging **25**(10), 1284–1295 (2006).
[21] G. T. Silva, S. G. Chen, J. F. Greenleaf, and M. Fatemi, "Dynamic ultrasound radiation force in fluids," Phys. Rev. E **71**(5), 056617 (2005).
[22] T. D. Rossing, R. F. Moore, and P. A. Wheeler, *The Science of Sound*, 3rd ed. (Addison Wesley, San Francisco, 2002), p. 47.